Spin Orientation and Magnetostriction of $Tb_{1-x}Dy_xFe_2$ from First Principles

Christopher E. Patrick,[1,*] George A. Marchant,[2] and Julie B. Staunton[2]

[1] *Department of Materials, University of Oxford, Parks Road, Oxford OX1 3PH, United Kingdom*
[2] *Department of Physics, University of Warwick, Coventry CV4 7AL, United Kingdom*

(Received 20 March 2020; revised 3 June 2020; accepted 13 July 2020; published 29 July 2020)

The optimal amount of dysprosium in the highly magnetostrictive rare-earth compounds $Tb_{1-x}Dy_xFe_2$ for room-temperature applications has long been known to be $x = 0.73$ (Terfenol-D). Here, we derive this value from first principles by calculating the easy magnetization direction and magnetostriction as a function of composition and temperature. We use crystal-field coefficients obtained within density-functional theory to construct phenomenological anisotropy and magnetoelastic constants. The temperature dependence of these constants is obtained from disordered-local-moment calculations of the rare-earth magnetic order parameter. Our calculations find the critical Dy concentration required to switch the magnetization direction at room temperature to be $x_c = 0.78$, with magnetostrictions $\lambda_{111} = 2700$ and $\lambda_{100} = -430$ ppm, close to the Terfenol-D values.

DOI: 10.1103/PhysRevApplied.14.014091

I. INTRODUCTION

The cubic Laves-phase compound Terfenol-D ($Tb_{1-x}Dy_xFe_2$, $x = 0.73$) has unparalleled magnetostrictive properties at room temperature, developing strains of 1600 ppm when a small magnetic field is applied and rotated between the [100] and [111] crystal directions [1–3]. Originally developed for sonar [4], Terfenol-D has a range of potential applications, including vibrational energy harvesting [5,6], nondestructive testing [7], and multiferroic devices [8]. The latter concept couples magnetostrictive and piezoelectric materials to control electric polarization (or magnetization) with a magnetic (or electric) field, which is essential for magnetic sensors or magnetoresistive memory [9].

While remarkable for its magnetostriction, Terfenol-D does suffer from two drawbacks: it is brittle [10] and, due to its reliance on the critical heavy rare earths (REs) Tb and Dy, it is expensive [11]. Intense research has been aimed at finding new materials with reduced or zero RE content and better mechanical properties, with the notable successes of Fe-Ga and Fe-Al (Galfenol and Alfenol) [12,13]. Computational modeling, adopting a first-principles (parameter-free) methodology, provides a complementary approach to experimentally searching for new materials, as well as understanding existing ones [14–19]. However, despite Terfenol-D's huge importance as a magnetostrictive material, first-principles modeling has not yet been able to answer a basic question: namely, why is the optimum dysprosium content $x = 0.73$?

Experimentally, the question can be answered by considering the spin-orientation phase diagram [20], which maps out the preferred (easy) direction of magnetization of $Tb_{1-x}Dy_xFe_2$ as a function of x and temperature T. At $T = 300$ K, for $x \leq 0.6$ the easy direction is along [111]; for $x \geq 0.9$, it is [100]. The critical concentration $x_c = 0.73$ lies within the soft boundary between these two regions of the phase diagram and corresponds to a low magnetocrystalline anisotropy (MCA). The low MCA is essential for the aforementioned applications, since then only a small field is needed to trigger a magnetostrictive response. It is also important to note that this critical concentration x_c reduces with temperature [20].

A first-principles understanding of Terfenol-D therefore requires calculation of the spin-orientation diagram. These have been calculated in the past using crystal-field (CF) theory [20–24], which, although giving physical insight, requires parameters from, e.g., experiment or point-charge models, which are difficult to fit. For instance, Ref. [22] demonstrates how three different sets of CF parameters can reproduce the same experimental magnetostriction curve for $DyFe_2$. First-principles calculations are free of these parameters but are often limited to describing stoichiometric compounds at zero temperature.

Here, we combine nonempirical first-principles calculations with the CF approach in order to calculate the spin-orientation diagram of $Tb_{1-x}Dy_xFe_2$ and the critical concentration $x_c(T)$. Our approach takes the recently introduced yttrium-analog method of calculating CF coefficients within density-functional theory (DFT) [25]—which is numerically stable and avoids problems traditionally associated with describing highly correlated $4f$ electrons

*christopher.patrick@materials.ox.ac.uk

in DFT—and extends it to compute the phenomenological model parameters associated with magnetostriction. CF theory is then used to calculate the magnetocrystalline and magnetoelastic energies associated with these localized RE-4f electrons. We further include the magnetostrictive contribution from itinerant electrons using the finite-temperature DFT-based formulation of the disordered-local-moment picture. Our calculated spin-orientation diagram reproduces experimental measurements of the [111] and [100] easy directions over the full range of temperatures and concentrations. We find the critical concentration x_c to be 0.78 at room temperature, with magnetostrictions $\lambda_{111} = 2700$ and $\lambda_{100} = -430$ ppm, close to the Terfenol-D values.

The rest of the paper is organized as follows. Section II describes the theory behind our calculation of the spin-orientation diagram. In particular, we introduce the phenomenological expression for the total energy as a function of the magnetization direction and strain and discuss the magnetocrystalline and magnetoelastic constants that enter this expression. We review how the contribution to these constants from RE-4f electrons can be connected to CF coefficients and describe how these coefficients are obtained within DFT. We also discuss the disordered-local-moment calculations used to obtain the itinerant electron contribution and the temperature dependence of the RE-4f magnetic moments. We then present our results in Sec. III, consisting of the calculated magnetocrystalline and magnetoelastic constants of $TbFe_2$ and $DyFe_2$ and then the composition and temperature-dependent spin-orientation diagram, which is the main result of this work. Finally, in Sec. IV, we outline future research directions.

II. METHODOLOGY

A. Spin orientation at zero temperature

Our calculations are based on the following phenomenological expression for the energy of the crystal,

$$E(\hat{\mathbf{e}}, \boldsymbol{\varepsilon}) = E_{\mathrm{el}}(\boldsymbol{\varepsilon}) + E_{\mathrm{RE}}(\hat{\mathbf{e}}, \boldsymbol{\varepsilon}) + E_{\mathrm{itin}}(\hat{\mathbf{e}}, \boldsymbol{\varepsilon}), \tag{1}$$

which consists of a magnetization-independent elastic energy E_{el}, a contribution E_{RE} originating from the 4f electrons localized on the RE atoms, and E_{itin}, which originates from itinerant (delocalized) electrons. $\boldsymbol{\varepsilon}$ represents the strain, with components written either in Cartesian form ($\varepsilon_{xx}, \varepsilon_{xy}$, etc.) or as linear combinations of these (ε^{α}, $\varepsilon^{\gamma i}$, $\varepsilon^{\epsilon i}$), where α, γ, and ϵ describe homogeneous, tetragonal, and shear-strain modes, respectively [26]. $\hat{\mathbf{e}}$ is a unit vector describing the orientation of the magnetization, which can alternatively be expressed as $\hat{\mathbf{e}} = (\cos\phi \sin\theta, \sin\phi \sin\theta, \cos\theta)$. The equilibrium strain and magnetization state is taken to be that which minimizes $E(\hat{\mathbf{e}}, \boldsymbol{\varepsilon})$.

The magnetization of the entire crystal can be seen as the sum of individual contributions from local magnetic moments, where each local moment with some magnitude μ is associated with a magnetic atom [27]. At zero temperature, the local moments form an ordered magnetic structure. Raising the temperature introduces thermal disorder amongst the local moments, which generally weakens the overall magnetization, until complete disorder is reached at the Curie temperature [27]. In the zero-temperature case, $\hat{\mathbf{e}}$ describes, equivalently, the orientation of a particular local moment *or* the orientation of the overall magnetization [28]. However, this equivalence does not hold at finite temperature, where the magnetic properties of the crystal are determined as an average over the fluctuating local moments. We concentrate initially on the zero-temperature case. The generalization to finite temperature is discussed in Sec. II F. We now discuss each term in Eq. (1).

1. Elastic energy

The elastic energy is quadratic in strain and depends on the three elastic constants c_{11}, c_{12}, and c_{44} [26,29]:

$$E_{\mathrm{el}}(\boldsymbol{\varepsilon}) = \frac{c_{11}}{2}(\varepsilon_{xx}^2 + \varepsilon_{yy}^2 + \varepsilon_{zz}^2) + c_{12}(\varepsilon_{yy}\varepsilon_{zz} + \varepsilon_{zz}\varepsilon_{xx} + \varepsilon_{xx}\varepsilon_{yy}) + \frac{c_{44}}{2}(\varepsilon_{xy}^2 + \varepsilon_{yz}^2 + \varepsilon_{zx}^2). \tag{2}$$

Ideally, we should calculate these constants from first principles. However, even obtaining zero-temperature elastic constants for the stoichiometric end compounds $TbFe_2$ and $DyFe_2$ in DFT is not straightforward due to the difficulty in treating the RE-4f electrons [30]. Furthermore, the elastic constants are, in principle, dependent on composition and temperature. For simplicity, we instead use a single set of elastic constant values of 141, 65, and 49 GPa for c_{11}, c_{12}, and c_{44}, for all compositions and temperatures. These values have been measured experimentally for $Tb_{0.3}Dy_{0.7}Fe_2$ [26]. We test the sensitivity of our results to this choice by calculating spin-orientation diagrams using different sets of elastic constant values, which are either obtained from DFT or measured experimentally, for different compositions [30,31]. The comparison is provided as an Appendix and shows the sensitivity to be very weak.

2. RE-4f electron energy

The energy associated with the RE-4f electrons $E_{\mathrm{RE}}(\hat{\mathbf{e}}, \boldsymbol{\varepsilon})$ can be further partitioned as

$$E_{\mathrm{RE}}(\hat{\mathbf{e}}, \boldsymbol{\varepsilon}) = E_{\mathrm{MCA}}(\hat{\mathbf{e}}) + E_{\mathrm{ME}}(\hat{\mathbf{e}}, \boldsymbol{\varepsilon}), \tag{3}$$

where the MCA energy $E_{\mathrm{MCA}}(\hat{\mathbf{e}})$ depends only on the orientation of the RE-4f magnetic moment and the magnetoelastic energy $E_{\mathrm{ME}}(\hat{\mathbf{e}}, \boldsymbol{\varepsilon})$ couples this orientation to the

strain. The MCA energy can be written as

$$E_{\mathrm{MCA}}(\hat{\mathbf{e}}) = \sum_{l=4,6} \mathcal{K}^{\alpha,l} S^{\alpha,l}(\hat{\mathbf{e}}), \tag{4}$$

where $\mathcal{K}^{\alpha,l}$ are the anisotropy constants and $S^{X,l}$ are the symmetry basis functions, which are listed in Ref. [26] ($X = \alpha, \gamma, \epsilon$). $\mathcal{K}^{\alpha,l}$ are related to the more conventional anisotropy constants K_1 and K_2 as $K_1 = -2(\mathcal{K}^{\alpha,4} + \frac{1}{22}\mathcal{K}^{\alpha,6})$ and $K_2 = \mathcal{K}^{\alpha,6}$.

The magnetoelastic energy $E_{\mathrm{ME}}(\hat{\mathbf{e}}, \boldsymbol{\varepsilon})$ is obtained as the direct product of strain and magnetization basis functions belonging to the same representation [26]:

$$\begin{aligned} E_{\mathrm{ME}}(\hat{\mathbf{e}}, \boldsymbol{\varepsilon}) = {} & \varepsilon^{\alpha} \sum_{l=4,6} \mathcal{B}^{\alpha,l} S^{\alpha,l}(\hat{\mathbf{e}}) \\ & + \sum_{i=1,2} \varepsilon^{\gamma i} \sum_{l=2,4,6} \mathcal{B}^{\gamma,l} S_i^{\gamma,l}(\hat{\mathbf{e}}) \\ & + \sum_{i=1,2,3} \varepsilon^{\epsilon i} \sum_{l=2,4,6,6'} \mathcal{B}^{\epsilon,l} S_i^{\epsilon,l}(\hat{\mathbf{e}}). \end{aligned} \tag{5}$$

The coefficients $\mathcal{B}^{X,l}$ are the magnetoelastic constants. Note how the lower symmetry of the tetragonal or shear-strained structures (γ or ϵ) generates new terms with an $l = 2$ dependence on magnetization direction.

Evaluation of $E_{\mathrm{RE}}(\hat{\mathbf{e}}, \boldsymbol{\varepsilon})$ therefore requires knowledge of the anisotropy and magnetoelastic constants $\mathcal{K}^{\alpha,l}$ and $\mathcal{B}^{X,l}$. We discuss the calculation of these constants within the framework of the single-ion model and CF theory in Secs. II B, II C, and II D.

3. Itinerant electron energy

The remaining term $E_{\mathrm{itin}}(\hat{\mathbf{e}}, \boldsymbol{\varepsilon})$ accounts for the MCA and magnetoelastic contributions to the energy not already included in the RE-4f term, i.e., those coming from itinerant electrons. These itinerant electrons are mainly Fe-3d in character, with a lesser contribution from the RE-5d electrons [14]. The relative importance of E_{RE} and E_{itin} to the magnetostriction can be assessed by comparing $TbFe_2$ or $DyFe_2$ to their isostructural counterpart $GdFe_2$. These three compounds have the same itinerant electronic structure and therefore should have comparable E_{itin}. However, E_{RE} is zero in $GdFe_2$ due to the filled Gd-4f spin subshell having zero orbital moment [32]. Comparing the experimentally measured magnetostrictions of the different compounds, we find that $TbFe_2$ has a magnetostriction that is 50 times larger than that for $GdFe_2$ [26], showing that E_{RE} is the dominant contribution to Eq. (1). Nevertheless, for completeness we still include E_{itin} in our analysis.

In principle, $E_{\mathrm{itin}}(\hat{\mathbf{e}}, \boldsymbol{\varepsilon})$ can be split into MCA and magnetoelastic contributions as in Eq. (3), with a different set of constants. In practice (Sec. III A), we find the MCA contribution to be negligible and also that it is sufficient only to consider the $l = 2$ term in the magnetoelastic expansion. We therefore have

$$E_{\mathrm{itin}}(\hat{\mathbf{e}}, \boldsymbol{\varepsilon}) = \mathcal{B}^{\gamma,2}_{\mathrm{itin}} \sum_{i=1,2} \varepsilon^{\gamma i} S_i^{\gamma,2}(\hat{\mathbf{e}}) + \mathcal{B}^{\epsilon,2}_{\mathrm{itin}} \sum_{i=1,2,3} \varepsilon^{\epsilon i} S_i^{\epsilon,2}(\hat{\mathbf{e}}). \tag{6}$$

Due to their itinerant electron origin, the constants $\mathcal{B}^{\gamma,2}_{\mathrm{itin}}$ and $\mathcal{B}^{\epsilon,2}_{\mathrm{itin}}$ cannot be obtained from CF theory. They are, however, amenable to treatment in the DFT-based disordered-local-moment picture [27,33]. We describe these calculations in Sec. II E.

B. Single-ion treatment of RE-4f contribution and modeling of alloys

We calculate the RE-4f energy $E_{\mathrm{RE}}(\hat{\mathbf{e}}, \boldsymbol{\varepsilon})$ within the single-ion model [34], which has been used to great effect to understand the behavior of RE-transition metal compounds for many years [32]. In this model, the magnetic moment associated with the 4f electrons localized on a particular RE ion behaves independently of its neighbors, which is a reasonable approximation [22] given the highly localized nature of these electrons and the relatively weak RE-RE magnetic interactions measured in neutron-scattering experiments [35]. The 4f electrons localized at different RE sites experience the same potential, which is an atomiclike central potential plus a contribution from the surrounding CF. The RE-4f electrons also all experience an exchange field originating from the itinerant electrons and possibly an external magnetic field, both of which drive the magnetic order [32].

The CF is supposed to derive from the valence electronic structure and therefore is insensitive to (a) the orientations of surrounding RE-4f localized moments and (b) the chemical species (Tb or Dy) of surrounding RE ions (since these species have the same $6s^2 5d$ valence electronic structure). This latter aspect allows a simple treatment of Tb-Dy alloying within the single-ion model, since each RE ion is independent: for a given composition $Tb_{1-x}Dy_xFe_2$, the RE-4f energy per ion is a superposition of the Tb and Dy contributions,

$$E_{\mathrm{RE}}(\hat{\mathbf{e}}, \boldsymbol{\varepsilon}) = (1-x)E_{\mathrm{Tb}}(\hat{\mathbf{e}}, \boldsymbol{\varepsilon}) + xE_{\mathrm{Dy}}(\hat{\mathbf{e}}, \boldsymbol{\varepsilon}), \tag{7}$$

where now E_{Tb} and E_{Dy} can be seen as the RE-4f energy contributions calculated for the end compounds $TbFe_2$ and $DyFe_2$, respectively. These end compounds each have their own set of two anisotropy and nine magnetoelastic constants, so to evaluate E_{RE} for an arbitrary x, we require 22 constants in total.

C. RE anisotropy and magnetoelastic constants from CF theory

In the single-ion central potential, the RE-4f electrons form atomiclike eigenstates $|L, S, J, M_J\rangle$, where L and S

are determined by Hund's rules, $J = L + S$ for Tb and Dy, and $M_J = J, J-1, \ldots, -J$ [36]. Now, we should construct a Hamiltonian for the RE-4f electrons including the crystal, exchange, and external fields, and diagonalize it within the manifold of states with different M_J [37]. Without the crystal and external fields, the ground state will be $|L,S,J,-J\rangle$, with the quantization axis (the magnetic moment direction) aligned with the exchange field. Taking this axis as $\hat{\mathbf{z}}$, the RE-4f electron density $\rho_{4f}^{(\hat{\mathbf{z}})}(\mathbf{r})$ associated with $|L,S,J,-J\rangle$ is given by [38]

$$\rho_{4f}^{(\hat{\mathbf{z}})}(\mathbf{r}) = n_{4f}^{0}(r) \sum_{l=2,4,6} \mathcal{A}_l \left(\frac{2l+1}{4\pi}\right)^{1/2} Y_{l0}(\hat{\mathbf{r}}). \quad (8)$$

Here, $n_{4f}^{0}(r)$ is the radial density calculated for the unperturbed central potential [32] and the $Y_{lm}(\hat{\mathbf{r}})$ are complex spherical harmonics. The $\mathcal{A}_l$ are RE-dependent numerical factors formed from J and Stevens coefficients, which for Tb^{3+} are $\mathcal{A}_2 = -(1/3)$, $\mathcal{A}_4 = (1/11)$, and $\mathcal{A}_6 = -(5/429)$, and for Dy^{3+} are $\mathcal{A}_2 = -(1/3)$, $\mathcal{A}_4 = -(4/33)$, and $\mathcal{A}_6 = (25/429)$ [38,39]. The RE-4f charge density $\rho_{4f}^{(\hat{\mathbf{e}})}(\mathbf{r})$ corresponding to a general magnetic moment direction $\hat{\mathbf{e}}$ is obtained from Eq. (8) by making the substitution $Y_{l0}(\hat{\mathbf{r}}) \to \sum_m e^{-im\phi} d_{m0}^{(l)}(\theta) Y_{lm}(\hat{\mathbf{r}})$, where the functions $d_{m0}^{(l)}(\theta)$ are equal to $[(l-m)!/(l+m)!]^{1/2} P_l^m(\cos\theta)$ and $P_l^m(x)$ are the associated Legendre polynomials [40].

The CF characterizes the nonspherical components of the potential at the RE site, $V(\mathbf{r}) = \sum_{lm} V_{lm}(r) Y_{lm}(\hat{\mathbf{r}})$. If the exchange field is sufficiently strong compared to the CF, the latter will not mix states of different M_J. Then, the energy shift due to the CF is obtained from first-order perturbation theory as

$$E_{4f}(\hat{\mathbf{e}}) = \sum_{l=2,4,6} \mathcal{A}_l \sum_m (-1)^m B_{l-m} e^{-im\phi} d_{m0}^{(l)}(\theta), \quad (9)$$

where the CF coefficients [25] have been introduced as

$$B_{lm} = \left(\frac{2l+1}{4\pi}\right)^{1/2} \int r^2 n_{4f}^{0}(r) V_{lm}(r)\, dr. \quad (10)$$

For $REFe_2$ in the cubic Laves phase (Fig. 1), the RE atoms sit at sites with T_d symmetry, so the only nonzero CF coefficients that appear in Eq. (9) are B_{40}, $B_{4\pm4}$, B_{60}, and $B_{6\pm4}$; only B_{40} and B_{60} are independent [41].

Here, we will assume that the exchange field is strong enough that $E_{4f}(\hat{\mathbf{e}})$ is given by Eq. (9) and also that the exchange field and magnetization are isotropic. Then, E_{4f} is the only contribution to the energy that depends on the magnetization angle. At zero strain, we can equate E_{4f} and

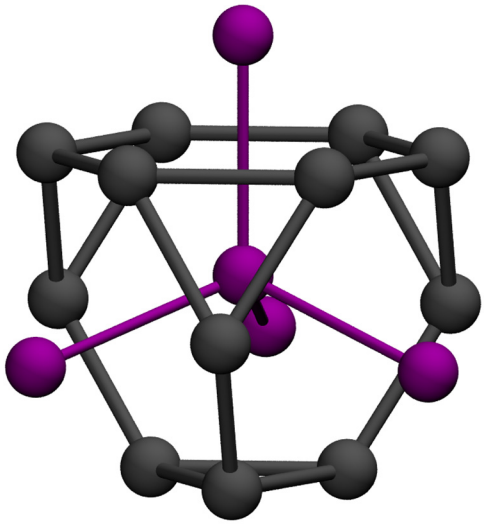

FIG. 1. The local T_d environment of the RE atom in the cubic Laves phase, showing nearest-neighbor (Fe, gray) and next-nearest-neighbor (RE, purple) atoms. The RE—RE bonds are oriented along the ⟨111⟩ directions.

E_{MCA} [Eqs. (4) and (9)] to obtain

$$\mathcal{K}^{\alpha,4} = \frac{5}{2}\mathcal{A}_4 B_{40}; \quad \mathcal{K}^{\alpha,6} = \frac{231}{2}\mathcal{A}_6 B_{60}. \quad (11)$$

Next, to obtain the magnetoelastic constants $\mathcal{B}^{X,l}$, we consider the modifications to the CF coefficients when three different strain modes are applied: $\varepsilon_{xx} = \varepsilon_{yy} = \varepsilon_{zz} = \varepsilon_I$ (isotropic), $\varepsilon_{zz} = -2\varepsilon_{xx} = -2\varepsilon_{yy} = \varepsilon_T$ (tetragonal), and $\varepsilon_{xy} = \varepsilon_{yz} = \varepsilon_{zx} = \varepsilon_S$ (shear). For the shear deformation, it is convenient to work in a rotated coordinate system where the z axis coincides with the [111] direction. Then, aside from altering the CF coefficients, which are already nonzero in the unstrained T_d environment, the tetragonal and shear strains affect $E_{4f}(\hat{\mathbf{e}})$ in Eq. (9) by generating a nonzero B_{20} coefficient.

Denoting the strain-induced shifts in CF coefficients as ΔB_{lm}, our calculations (Sec. III A) find that these shifts can be described well by the linear relation $\Delta B_{lm} = (dB_{lm}/d\varepsilon_X)\varepsilon_X$. Insertion of these relations into Eq. (9) and comparison with Eq. (5) gives each magnetoelastic constant in terms of the strain derivative of a CF coefficient, for instance,

$$\mathcal{B}^{\gamma,2} = \frac{2}{3}\mathcal{A}_2 \frac{dB_{20}}{d\varepsilon_T}; \quad \mathcal{B}^{\epsilon,2} = \mathcal{A}_2 \frac{dB_{20}}{d\varepsilon_S}. \quad (12)$$

D. DFT calculation of CF coefficients

Equations (11) and (12) show how the anisotropy and magnetoelastic constants can be obtained from the CF coefficients B_{lm} and their strain derivatives $dB_{lm}/d\varepsilon_X$. These are the quantities that we calculate from first principles within the yttrium-analog method [25]. In this

approach, the potential $V(\mathbf{r})$ that determines the CF coefficients is calculated within DFT for the "Y-analog" of $TbFe_2$ or $DyFe_2$, which is YFe_2. Specifically, the components $V_{lm}(r)$ in Eq. (10) are found from the angular decomposition of the self-consistent Kohn-Sham potential calculated for the desired $REFe_2$ structure, where the RE is replaced with Y.

We have previously used the Y-analog method to calculate CF coefficients for various RE–transition-metal compounds [25], demonstrating its applicability to describe temperature- and pressure-induced spin-reorientation transitions in the $RECo_5$ compounds [37,42,43]. Substitution of Tb or Dy with Y to calculate the CF is consistent with the assumptions of the single-ion model [34], namely that the CF depends on the valence electronic structure and not on the RE-4f electrons themselves. Since the RE ions are in the 3+ state and therefore are isovalent (two s and a single d electron), we expect the CF of YFe_2 to be a good approximation for $TbFe_2$ or $DyFe_2$. Indeed, use of the Y-analog ensures that there is no double counting of the RE-4f electrons in Eq. (10). Any DFT implementation can be used to calculate the CF coefficients, provided that the valence charge density is described accurately.

Equation (10) also contains the RE-4f electron density calculated for the unperturbed central potential $n^0_{4f}(r)$. Previously, we have calculated $n^0_{4f}(r)$ within self-interaction-corrected DFT [44,45] for a number of compounds and found that, for a given RE element, it is highly insensitive to the crystalline environment [25]. Therefore when calculating CF coefficients, we use the same previously calculated RE-dependent functions [$n^0_{4f,\mathrm{Tb}}(r)$ or $n^0_{4f,\mathrm{Dy}}(r)$ [46]] for all strain states.

E. Itinerant electron contribution

The itinerant electrons are (by definition) delocalized and are responsible for generating the CF rather than simply being influenced by it. Accordingly, the CF picture is not appropriate to describe their contribution to the magnetostriction. However, itinerant electron magnetism is amenable to a fully first-principles treatment within DFT [27]. In Sec. II A 3, we use $GdFe_2$ as a comparison system to understand the importance of $E_{\mathrm{itin}}(\hat{\mathbf{e}}, \boldsymbol{\varepsilon})$ to the magnetostriction, since it has the same valence electronic structure but zero CF contribution from the filled Gd-4f spin subshell. Building on this idea, we take $E_{\mathrm{itin}}(\hat{\mathbf{e}}, \boldsymbol{\varepsilon})$ to be the same for $Tb_{1-x}Dy_xFe_2$ and $GdFe_2$ and calculate the latter directly. Similarly to using the Y analog, this approach avoids any double counting of the CF contribution. However, the use of Gd rather than Y to calculate E_{itin} has the advantage of capturing any additional on-site polarization of the valence electrons by the large spin moments possessed by Gd, Tb, and Dy [47,48].

We calculate $E_{\mathrm{itin}}(\hat{\mathbf{e}}, \boldsymbol{\varepsilon})$ for $GdFe_2$ using the same method demonstrated recently for bcc Fe and Fe-Ga alloys [33]. This approach is a Green's function multiple-scattering theory-based formulation of the disordered-local-moment picture within DFT (DFT-DLM [27]), which—as discussed in Sec. II F—allows for the treatment of finite-temperature magnetic disorder. The filled Gd-4f spin subshell is treated efficiently using the local self-interaction correction (LSIC) [44]. Quantities related to the magnetic anisotropy are obtained by solving the relativistic single-site scattering problem and applying the torque method [49]. As described in Ref. [33], calculation of the derivative of the total energy with respect to the magnetization angle for different strain states allows the anisotropy and magnetoelastic constants to be obtained.

F. Generalization to finite temperature

The methodology described above is sufficient to evaluate Eq. (1) assuming that all the individual magnetic moments are ordered, corresponding to zero temperature. At finite temperature T, Eq. (1) takes a slightly different form:

$$E(\hat{\mathbf{n}}, \boldsymbol{\varepsilon}, T) = E_{\mathrm{el}}(\boldsymbol{\varepsilon}) + E_{\mathrm{RE}}(\hat{\mathbf{n}}, \boldsymbol{\varepsilon}, T) + E_{\mathrm{itin}}(\hat{\mathbf{n}}, \boldsymbol{\varepsilon}, T). \quad (13)$$

The new quantity introduced is the unit vector $\hat{\mathbf{n}}$, which describes the orientation of the magnetization of the entire crystal and therefore represents an average over the individual magnetic moments. The degree of magnetic order is quantified through the temperature-dependent order parameters m_{Tb}, m_{Dy}, and m_{itin}, which take values between 1 (zero temperature, fully ordered) and 0 (above the Curie temperature, fully disordered). The relationship between the orientation of the individual moments and their average is given by, for instance, $\langle \hat{\mathbf{e}}_{\mathrm{Tb}} \rangle_T = m_{\mathrm{Tb}}(T)\hat{\mathbf{n}}$, where $\langle\rangle_T$ denotes the statistical mechanical thermal average taken (in this example) over the individual moments of all Tb ions. More generally, the finite- and zero-temperature energies in Eqs. (1) and (13) are related simply as $E(\hat{\mathbf{n}}, \boldsymbol{\varepsilon}, T) = \langle E(\hat{\mathbf{e}}, \boldsymbol{\varepsilon}) \rangle_T$.

Evaluation of the thermal average $\langle\rangle_T$ requires a model for the statistical mechanics of the magnetic moments. The DFT-DLM framework employs a Heisenberg-like Hamiltonian for this purpose [27]. The probability that a moment is aligned along a direction $\hat{\mathbf{e}}$ at T is given by $P_{\hat{\mathbf{n}}}(\hat{\mathbf{e}}) \propto \exp[\beta h \hat{\mathbf{n}} \cdot \hat{\mathbf{e}}]$, where $1/\beta = k_B T$. The Weiss field felt by each local moment $h(T)$ is determined self-consistently from DFT-DLM calculations at a given temperature using the iterative scheme described in Ref. [50]. The self-consistency condition ensures (a) that the free energy is minimized and (b) that the model approximates the true statistical mechanics of the moments as closely as possible [27]. Each crystallographically inequivalent magnetic atom (Tb, Dy, and Fe) experiences its own Weiss field and within the model the order parameter and Weiss fields are

linked according to (again taking Tb as an example):

$$m_{\mathrm{Tb}}(T) = \coth(\beta h_{\mathrm{Tb}}(T)) - \frac{1}{\beta h_{\mathrm{Tb}}(T)}. \tag{14}$$

1. Thermally averaged rare-earth contribution

Recalling that, in the CF picture, the CF is independent of the RE moment orientations and that the anisotropy and magnetoelastic constants are determined by the CF coefficients, the thermal average of the RE contribution is determined by solely by the average of the symmetry basis functions, e.g.,

$$E_{\mathrm{MCA}}(\hat{\mathbf{n}}, T) = \sum_{l=4,6} \mathcal{K}^{\alpha,l} \langle S^{\alpha,l}(\hat{\mathbf{e}}) \rangle_T. \tag{15}$$

Due to the local nature of the probability function $P_{\hat{\mathbf{n}}}(\hat{\mathbf{e}})$, the general arguments of Callen and Callen [34] can be used to show that

$$\langle S^{X,l}(\hat{\mathbf{e}}) \rangle_T = f_l(m) S^{X,l}(\hat{\mathbf{n}}), \tag{16}$$

where the functions $f_l(m)$ depend on m as $m^{[l(l+1)]/2}$ and m^l at low and high temperature, respectively [34]. Then, the explicit expression for the RE contribution at finite temperature is

$$\begin{aligned} E_{\mathrm{RE}}(\hat{\mathbf{n}}, \boldsymbol{\varepsilon}, T) = & \sum_{l=4,6} \mathcal{K}^{\alpha,l}_{\mathrm{RE}}(T) S^{\alpha,l}(\hat{\mathbf{n}}) \\ & + \varepsilon^{\alpha} \sum_{l=4,6} \mathcal{B}^{\alpha,l}_{\mathrm{RE}}(T) S^{\alpha,l}(\hat{\mathbf{n}}) \\ & + \sum_{i=1,2} \varepsilon^{\gamma i} \sum_{l=2,4,6} \mathcal{B}^{\gamma,l}_{\mathrm{RE}}(T) S^{\gamma,l}_i(\hat{\mathbf{n}}) \\ & + \sum_{i=1,2,3} \varepsilon^{\epsilon i} \sum_{l=2,4,6,6'} \mathcal{B}^{\epsilon,l}_{\mathrm{RE}}(T) S^{\epsilon,l}_i(\hat{\mathbf{n}}), \end{aligned} \tag{17}$$

where the finite and zero-temperature constants are simply related by f_l,

$$\begin{aligned} \mathcal{K}^{\alpha,l}_{\mathrm{RE}}(T) &= \mathcal{K}^{\alpha,l}_{\mathrm{RE}} f_l(m_{\mathrm{RE}}(T)), \\ \mathcal{B}^{X,l}_{\mathrm{RE}}(T) &= \mathcal{B}^{X,l}_{\mathrm{RE}} f_l(m_{\mathrm{RE}}(T)), \end{aligned} \tag{18}$$

and the RE subscript is inserted as a reminder that the constants and order parameters are calculated either for $TbFe_2$ or $DyFe_2$. The RE contribution for the $Tb_{1-x}Dy_xFe_2$ alloy is obtained through the same linear mixing as at zero temperature, as in Eq. (7).

The temperature dependence of $E_{\mathrm{RE}}(\hat{\mathbf{n}}, \boldsymbol{\varepsilon}, T)$ is therefore fixed by the order-parameter dependencies $m_{\mathrm{Tb}}(T)$ and $m_{\mathrm{Dy}}(T)$, which we determine through finite-temperature LSIC DFT-DLM calculations on $TbFe_2$ and $DyFe_2$. The calculations are performed according to the methodology described in detail in Ref. [48] and the reader is referred there for a more complete discussion of the underlying theory and technical details of the DFT-DLM scheme.

2. Thermally averaged itinerant electron contribution

Performing the thermal average on E_{itin} gives, in analogy with Eq. (17),

$$\begin{aligned} E_{\mathrm{itin}}(\hat{\mathbf{n}}, \boldsymbol{\varepsilon}, T) = & \mathcal{B}^{\gamma,2}_{\mathrm{itin}}(T) \sum_{i=1,2} \varepsilon^{\gamma i} S^{\gamma,2}_i(\hat{\mathbf{n}}) \\ & + \mathcal{B}^{\epsilon,2}_{\mathrm{itin}}(T) \sum_{i=1,2,3} \varepsilon^{\epsilon i} S^{\epsilon,2}_i(\hat{\mathbf{n}}). \end{aligned} \tag{19}$$

The finite-temperature magnetoelastic constants are obtained from DFT-DLM calculations on $GdFe_2$, which give the temperature dependence of $\mathcal{B}^{X,2}_{\mathrm{itin}}$ directly. As found previously for bcc Fe [33], the $\mathcal{B}^{X,2}_{\mathrm{itin}}$ constants do not follow an $f_2(m_{\mathrm{itin}})$ dependence on the order parameter. This observation reflects the itinerant origin of the magnetic anisotropy, compared to the single-ion description of the RE moments [49].

3. The need for a phenomenological model

It is reasonable to ask, given that LSIC DFT-DLM calculations can be used to obtain the itinerant electron magnetostriction and also the temperature dependence of the RE order parameters in $TbFe_2$ and $DyFe_2$, why we should not perform the entire calculation in the DFT-DLM framework without any reference to CF theory. The technical difficulty is that the DFT-DLM calculations are performed within the atomic sphere approximation (ASA) [51], which means that nonspherical components of the potential at the RE site (i.e., the CF) are poorly described in the DFT-DLM calculation of the RE anisotropy. As a result, a separate treatment of the CF is required. In turn, it is important that the calculated energy contribution associated with the itinerant electron anisotropy is free of any contribution from the localized RE-4f electrons interacting with the CF; otherwise, this contribution would be counted both in E_{itin} and E_{RE} in Eq. (1). Calculation of the itinerant contribution for $GdFe_2$, which has no CF anisotropy, ensures that this is the case. Similarly, the assumptions of the CF model mean that the CF coefficients themselves should not depend on the asphericity of the RE-4f electrons. This requirement is satisfied by using the Y-analog model, where the RE-4f electrons do not enter the calculation of the CF potential at all [25]. These same considerations have led us to adopt a similar scheme in the calculation of finite-temperature anisotropy of the RCo_5 compounds [37].

G. Computational details

The CF coefficients are calculated for YFe_2 within the projector-augmented formulation of DFT as implemented in the GPAW code [52], using the local spin-density approximation (LSDA) for exchange and correlation [53]. A plane-wave basis set with a 1200-eV energy cutoff and $20 \times 20 \times 20$ k-point sampling is used, as in Ref. [25]. A lattice constant of 7.341 Å is used throughout for the equilibrium (cubic) structure, which is the experimentally measured value for $TbFe_2$ at room temperature [54]; the value for $DyFe_2$ is very similar (7.338 Å). The dependence of the order parameters on the temperature is calculated within DFT-DLM [27] with the LSIC applied [48], using the ASA with Wigner-Seitz radii of 1.90 Å for the RE atoms, with angular-momentum expansions truncated at $l_{\max} = 3$. The same computational setup is used to calculate the temperature-dependent magnetoelastic constants associated with the itinerant electrons for $GdFe_2$, using the torque method as described in Refs. [33] and [49].

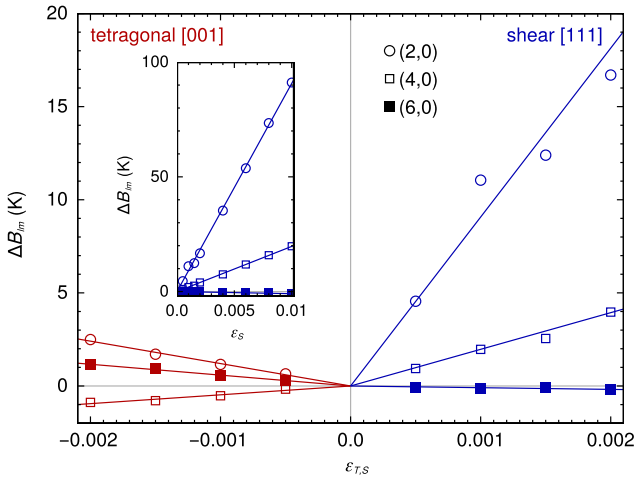

FIG. 2. The change in the CF coefficients ΔB_{lm} for $TbFe_2$ for different (l, m) with a shear strain ε_S (blue) or a tetragonal strain ε_T (red) applied. The inset shows ΔB_{lm} for a larger variation in ε_S. The straight lines are fits to the calculations.

III. RESULTS

A. Anisotropy and magnetoelastic constants

We have previously reported Y-analog calculations of the CF coefficients of $TbFe_2$ and $DyFe_2$ [25]. The values of $\mathcal{K}^{\alpha,4}$ and $\mathcal{K}^{\alpha,6}$ calculated from Eq. (11) are given in Table I. Importantly, due to the differences in $\mathcal{A}_4$ and $\mathcal{A}_6$ for Tb^{3+} and Dy^{3+}, $\mathcal{K}^{\alpha,l}$ have opposite signs for $TbFe_2$ and $DyFe_2$ and so favor different magnetization directions. From the linear mixing of Eq. (7), we note that a Dy content of $x = 0.45$ would lead to a zero value of $\mathcal{K}^{\alpha,4}$.

Now considering the magnetoelastic constants associated with the RE, in Fig. 2 we plot the strain-induced change in the CF coefficients ΔB_{lm} for $TbFe_2$, for $(l, m) = (2, 0)$, (4,0) and (6,0). We show ΔB_{lm} for both tetragonal (ε_T) and shear (ε_S) strains. Following convention, we divide the CF coefficients by k_B so that the quantities have dimensions of temperature.

Although there is some numerical noise in ΔB_{20} evident for small shear strains ε_S, ΔB_{lm} is linear in ε over the range of strains considered. Indeed, extending the calculations to larger shear strains confirms this linear relation out to at least $\varepsilon_S = 0.01$ (inset of Fig. 2). Then, the most striking feature of Fig. 2 is the strong dependence of B_{20} on ε_S. At $\varepsilon_S = 0.002$, ΔB_{20} is 17 K, compared to 2 K for ε_T at -0.002. The corresponding difference between the shear and tetragonal strains is much reduced at larger (l, m) values, with $\Delta B_{40} = 4$ K and -1 K and $\Delta B_{60} = 0$ K and 1 K, respectively.

Conversion of these derivatives into magnetoelastic constants through relations such as Eq. (12) gives the values shown in Table I. The large value of $dB_{20}/d\varepsilon_S$ is reflected in the coefficient $\mathcal{B}^{\epsilon,2}$, which is an order of magnitude larger than $\mathcal{B}^{\gamma,2}$. Since $\mathcal{B}^{\epsilon,2}$ is negative, this term will favor positive strains along [111]. Furthermore, $\mathcal{B}^{\epsilon,2}$ is the same sign for both $TbFe_2$ and $DyFe_2$, since $\mathcal{A}_2$ is identical for Tb^{3+} and Dy^{3+} [38,39]. Therefore, unlike $\mathcal{K}^{\alpha,4}$, there is no cancellation of $\mathcal{B}^{\epsilon,2}$ in the alloy. It is this aspect that allows $Tb_{1-x}Dy_xFe_2$ to have, simultaneously, a large magnetostriction and small anisotropy.

Now considering the itinerant electrons, our DFT-DLM calculations on $GdFe_2$ find the contribution to the MCA to be negligible (of order 1 Jm^{-3}). The magnetoelastic constants are more significant and their zero-temperature values are given in Table I (we stress again that their temperature dependence is more complicated than $f_l(m)$) [33]. The magnetoelastic contribution is well described by constants with $l = 2$ only. $\mathcal{B}^{\gamma,2}_{\mathrm{Fe}}$ and $\mathcal{B}^{\epsilon,2}_{\mathrm{Fe}}$ are calculated to have the same sign as observed experimentally for bcc Fe [55] but their magnitudes are enhanced (-7.1 and 33 MJ m^{-3}). However, the itinerant electrons still contribute much less than the RE at all of the temperatures considered here.

B. Easy directions and magnetostrictions at zero temperature

Using the constants reported in Table I, we can construct the phenomenological energy for an arbitrary strain, magnetization, and composition. Considering the zero-temperature case first [Eq. (1)], minimization of $E(\hat{\mathbf{e}}, \boldsymbol{\varepsilon})$ with respect to the magnetization direction and strain for the end compounds $TbFe_2$ and $DyFe_2$ finds easy directions of [111] and [100], respectively. The calculated fractional changes in length along [111] and [100] for $TbFe_2$ and $DyFe_2$ are $\lambda_{111}^{\mathrm{TbFe_2}} = 5200$ ppm and $\lambda_{100}^{\mathrm{DyFe_2}} = -780$ ppm at 0 K. A comparison with experimentally measured values of 4400 and -70 ppm [3] shows correct qualitative behavior and numerical agreement within approximately 1000

TABLE I. Anisotropy and magnetoelastic constants in MJ m^{-3}, calculated for $TbFe_2$ and $DyFe_2$.

	$\mathcal{K}^{\alpha,4}$	$\mathcal{K}^{\alpha,6}$	$\mathcal{B}^{\alpha,4}$	$\mathcal{B}^{\alpha,6}$	$\mathcal{B}^{\gamma,2}$	$\mathcal{B}^{\gamma,4}$	$\mathcal{B}^{\gamma,6}$	$\mathcal{B}^{\epsilon,2}$	$\mathcal{B}^{\epsilon,4}$	$\mathcal{B}^{\epsilon,6}$	$\mathcal{B}^{\epsilon,6'}$	$\mathcal{B}^{\gamma,2}_{\text{itin}}$	$\mathcal{B}^{\epsilon,2}_{\text{itin}}$
$TbFe_2$	14.10	11.20	−22.87	−27.88	74.69	28.08	6.96	−844.24	258.17	7.22	−4.20	−7.25	33.24
$DyFe_2$	−17.34	−47.52	28.14	116.89	77.12	−30.87	−29.43	−794.88	−307.96	−33.07	17.79	−7.25	33.24

ppm, or 0.1% strain; in relative terms, the agreement for $\lambda_{100}^{DyFe_2}$ is less good than for $TbFe_2$.

Now considering the alloy through Eq. (7), we find a [111] easy direction for all values of x below $x_c = 0.56$, above which the easy direction switches abruptly to [100]. This is some way off the experimental optimal concentration of $x = 0.73$ but we have not yet included temperature effects. It is also interesting to recompute the magnetization direction ignoring the magnetoelastic contribution to the energy. Then, x_c is found to be 0.45, the same value that cancelled $\mathcal{K}^{\alpha,4}$.

C. Spin-orientation diagram

We now consider finite temperature and minimize $E(\hat{\mathbf{n}}, \boldsymbol{\epsilon}, T)$ [Eq. (13)] for a grid of (x, T) values. The resulting spin-orientation diagram is shown in Fig. 3. As at zero temperature, the easy directions are found either to be [111] or [100] (blue or red regions) and increased Dy content favors [100] magnetization. However, at higher temperatures more Dy is required to maintain the [100] magnetization, i.e., x_c increases with temperature.

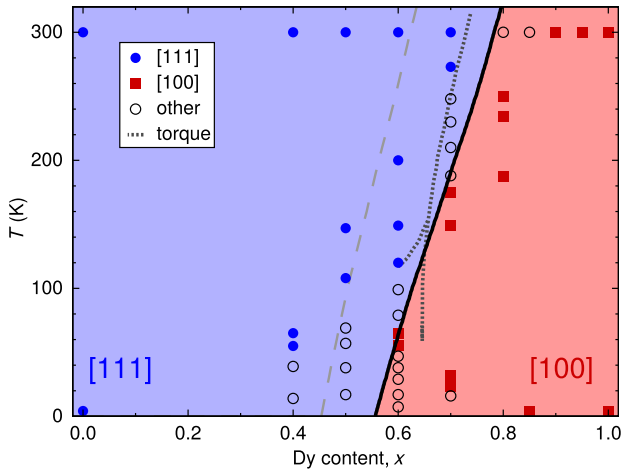

FIG. 3. The easy direction of magnetization of $Tb_{1-x}Dy_xFe_2$, calculated by minimizing $E(\hat{\mathbf{n}}, \boldsymbol{\epsilon}, x, T)$ (red- and blue-shaded regions). The symbols are experimental measurements of the easy direction using Mössbauer spectroscopy [20,56]. The dotted lines mark the boundaries between different magnetization directions extracted from torque magnetometry [57], where above 150 K the boundary is between [111] and [100] and below encloses a region of intermediate magnetization direction. The dashed line is the [111]-[100] boundary obtained by minimizing E_{MCA} only.

The reason for the increase in x_c is the behavior of the RE order parameters with temperature. Our DFT-DLM calculations find that the Dy order parameter m_{Dy} decreases more quickly with T than m_{Tb}, something that can also be inferred from experimental magnetization measurements [26]. This behavior can be understood as the lower spin moment of Dy weakening the exchange interaction [14]. Since $\mathcal{K}^{\alpha,4}$ is highly sensitive to m [approximately m^{10}, due to $f_4(m)$], more Dy is required at higher temperatures to maintain the [100] magnetization.

Our calculated value of x_c at 300 K is $x_c = 0.78$. At this concentration, we calculate magnetostrictions of $\lambda_{111} = 2700$ and $\lambda_{100} = -430$ ppm. As at zero temperature with the end compounds, the calculated values are within approximately 1000 ppm of the experimental ones, as measured at 300 K for Terfenol-D [1].

As for the zero-temperature case, we also calculate the spin orientation ignoring the magnetoelastic terms in the energy. The boundary between the [111] and [100] easy directions in this case is shown as the gray dashed line in Fig. 3. The shifted line can be understood from Fig. 2 and the surrounding discussion: $\mathcal{B}^{\epsilon,2}$ is large, so while the magnetization points along [111], the material can save energy by distorting. Switching off the magnetoelastic contribution reduces the region where [111] magnetization is favorable, so less Dy is required to make the transition to [100].

Figure 3 also shows experimental measurements of the easy magnetization direction obtained from Mössbauer spectroscopy [20,56] and torque-magnetometry measurements of the (x, T) boundaries between different magnetization orientations [57]. Our calculations agree with all of the measurements of the [111] and [100] easy directions across different temperatures and compositions (no red symbols appear on blue and vice versa). However, the open circles in Fig. 3 are measurements where the magnetization points along $[uv0]$ or $[uvw]$ rather than [111] or [100] [56]. Our calculations do not capture these intermediate directions, as we shall discuss in the concluding section.

IV. OUTLOOK

We first return to the original question of our work concerning Terfenol-D's optimum dysprosium content, $x = 0.73$. Our calculations actually find that the entire composition range of $Tb_{1-x}Dy_xFe_2$ is remarkable for having highly anisotropic magnetostrictions. For instance, we find

TABLE II. Elastic constants, in gigapascals either measured experimentally (exp.) or calculated (calc.) for different compounds.

	c_{11}	c_{12}	c_{44}
$Tb_{0.3}Dy_{0.7}Fe_2$, exp. [26]	141	65	49
$DyFe_2$, exp. [26]	146	68	47
$TbFe_2$, calc. [30]	197	112	84
YFe_2, calc. [31]	206	132	50

that the end compounds have $\lambda_{111}^{DyFe_2} = 5640$ and $\lambda_{100}^{TbFe_2} = -970$ ppm at 0 K (compare with $\lambda_{111}^{TbFe_2} = 5200$ ppm and $\lambda_{100}^{DyFe_2} = -780$ ppm reported above). However, what is critical for applications is the ability to rotate the magnetization direction at small fields [26], i.e., a small MCA, which is achieved at x_c, where the easy direction switches. Our calculated value of $x_c = 0.78$ at 300 K rationalizes the experimentally determined critical concentration from first principles. We stress that we get a very different value if we ignore temperature ($x_c = 0.56$) or magnetostriction ($x_c = 0.62$).

Interestingly, our calculations do not capture a more subtle feature of the spin-orientation diagram, which is the presence of $[uv0]$ or $[uvw]$ easy magnetization directions (open circles in Fig. 3) [56]. The reason for this discrepancy is in our first-order treatment of the CF, which generates terms up to $l = 6$ in Eq. (1). In order to describe $[uv0]$ or $[uvw]$ easy directions, the energy must contain terms with larger l [24,58]. To proceed, we should go beyond the first-order perturbative treatment of the CF [Eq. (9)] and instead construct the full RE-4f Hamiltonian, including the CF potential and the exchange field, and diagonalize it within the M_J manifold [37]. A complete treatment would map out the strain dependence of all terms within the Hamiltonian. This approach could potentially find intermediate easy directions and also allow us to calculate the dependence of $Tb_{1-x}Dy_xFe_2$ magnetostriction on the external field. Our test calculations using a finite exchange field indeed find intermediate easy directions for small T and $x \sim 0.5$, indicating that this is a promising direction for future work.

A further refinement is to account for internal distortions within the unit cell. Indeed, the classic work of Cullen and Clark [59] argued that the internal distortion could provide the key to explaining the huge anisotropy in magnetostriction between the [111] and [100] directions. However, as shown by the zero-temperature calculations of Ref. [16] and reiterated here, λ_{111} is found to be much larger than λ_{100} even when no internal distortions are taken into account. Our test calculations of the CF coefficients along different frozen phonon modes find the variation to be small compared to applying a global strain. However, the (zero-temperature) calculations of Ref. [16] did find a reduction in $\lambda_{111}^{TbFe_2}$ of 1300 ppm when they included an internal distortion, which would bring our value closer to experiment. Therefore, it is important to investigate the inclusion of all possible distortions and couplings at a consistent level.

An additional question concerns the use of the single-ion approximation [e.g., Eq. (7)]. This approximation is generally understood to work very well for RE–transition-metal magnets such as $REFe_2$ [32]. However, it is reasonable to ask to what extent the CF parameters and the exchange field at the RE site might be influenced by fluctuations in its surroundings, including those caused by other RE atoms. The application of our methodology to supercells incorporating such fluctuations will allow this question to be addressed.

Going beyond Terfenol-D, having validated the methodology, we can now evaluate the magnetostrictive properties of other materials, ideally with reduced RE content. The ability to calculate phase boundaries is of particular interest to the design of multiferroic architectures, where working at such boundaries will maximize the response [9]. For instance, we could easily simulate epitaxial strain by adding additional strain to our calculations or, more ambitiously, model the explicit effects of the interface on the CF. Intriguingly, the calculations also show that there exists a basic property of the Laves-phase structure, perhaps the orientation of RE—RE bonds, which makes the CF highly sensitive to shear strain. Elucidation of this mechanism could help in the design of more magnetostrictive materials.

ACKNOWLEDGMENTS

The present work forms part of the PRETAMAG project, funded by the United Kingdom Engineering and Physical Sciences Research Council, Grant No. EP/M028941/1.

APPENDIX: ELASTIC CONSTANTS

In our calculations of the elastic energy (Sec. II A 1), we use the values of the elastic constants c_{11}, c_{12} and c_{44} measured experimentally [26] for $Tb_{0.3}Dy_{0.7}Fe_2$ for all compositions and temperatures. Here, we illustrate the effect on the spin-orientation diagram of using different values for these constants. Table II lists elastic constants either measured experimentally for $Tb_{0.3}Dy_{0.7}Fe_2$ and $DyFe_2$ [26] or calculated within DFT for $TbFe_2$ and YFe_2 [30,31]. For the DFT calculations, a generalized-gradient approximation (GGA) is used for the exchange correlation. We include YFe_2 due to it having the same valence electronic structure.

We recalculate the spin-orientation diagram for each set of constants and show the result in Fig. 4. The qualitative

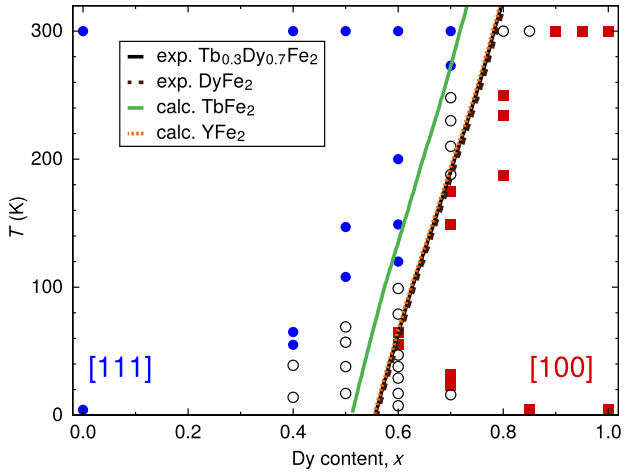

FIG. 4. The spin-orientation diagram of $Tb_{1-x}Dy_xFe_2$ calculated with different sets of elastic constants. The same experimental data are shown as in Fig. 3. The diagonal lines represent the boundaries between [111] and [100] directions of magnetization for the different sets of elastic constants listed in Table II.

structure of the diagram for each set of constants is identical, consisting of a single boundary between the [111] and [100] easy directions. Quantitatively, the three sets of elastic constants corresponding to $Tb_{0.3}Dy_{0.7}Fe_2$ and $DyFe_2$ (experimental) and YFe_2 [30,31] (calculated) give effectively identical boundaries. Use of the elastic constants calculated for $TbFe_2$ shifts the critical concentration x_c down by approximately 0.05, such that $x_c = 0.51$ at 0 K and $x_c = 0.72$ at 300 K. Examination of Table II would indicate that the critical concentration is most sensitive to c_{44}, which is reasonable given the crucial role played by the large [111] magnetostriction.

We note that using the elastic constants calculated for $TbFe_2$ brings the room-temperature critical concentration to within 0.01 of the experimental Terfenol-D value. However, since it is not clear that a GGA treatment is sufficiently accurate to describe the Tb-4*f* electrons [30,48], in this work we prefer to use experimental values for the elastic constants. Furthermore, the effectively identical results for $Tb_{0.3}Dy_{0.7}Fe_2$ and $DyFe_2$—and the weak sensitivity to c_{ij} in general—justifies the use of a single set of elastic constants for the entire spin-orientation diagram.

[1] R. Abbundi and A. Clark, Anomalous thermal expansion and magnetostriction of single crystal $Tb_{0.27}Dy_{0.73}Fe_2$, IEEE Trans. Magn. **13**, 1519 (1977).

[2] A. E. Clark, High-field magnetization and coercivity of amorphous rare-earth-Fe_2 alloys, Appl. Phys. Lett. **23**, 642 (1973).

[3] A. Clark, R. Abbundi, H. Savage, and O. McMasters, Magnetostriction of rare earth-Fe_2 Laves phase compounds, Physica B+C **86–88**, 73 (1977).

[4] E. du Trémolet de Lacheisserie, *Magnetostriction: Theory and Applications of Magnetoelasticity* (CRC Press, Boca Raton, FL, 1993).

[5] M. E. Staley and A. B. Flatau, in *Smart Structures and Materials 2005: Smart Structures and Integrated Systems*, edited by A. B. Flatau, International Society for Optics and Photonics Vol. 5764 (SPIE, 2005), p. 630–640.

[6] Z. Deng and M. J. Dapino, Review of magnetostrictive vibration energy harvesters, Smart Mater. Struct. **26**, 103001 (2017).

[7] J. Rudd and O. Myers, Experimental fabrication and nondestructive testing of carbon fiber beams for delaminations using embedded Terfenol-D particles, J. Intell. Mater. Syst. Struct. **29**, 600 (2018).

[8] Q. Wang, X. Li, C.-Y. Liang, A. Barra, J. Domann, C. Lynch, A. Sepulveda, and G. Carman, Strain-mediated 180° switching in CoFeB and Terfenol-D nanodots with perpendicular magnetic anisotropy, Appl. Phys. Lett. **110**, 102903 (2017).

[9] D. Li, X.-M. Zhao, H.-X. Zhao, X.-W. Dong, L.-S. Long, and L.-S. Zheng, Construction of magnetoelectric composites with a large room-temperature magnetoelectric response through molecular-ionic ferroelectrics, Adv. Mater. **30**, 1803716 (2018).

[10] J. Atulasimha and A. B. Flatau, A review of magnetostrictive iron-gallium alloys, Smart Mater. Struct. **20**, 043001 (2011).

[11] J. D. S. Vincent, M. Rodrigues, Z. Leong, and N. A. Morley, Design and development of magnetostrictive actuators and sensors for structural health monitoring, Sensors **20**, 711 (2020).

[12] A. E. Clark, K. B. Hathaway, M. Wun-Fogle, J. B. Restorff, T. A. Lograsso, V. M. Keppens, G. Petculescu, and R. A. Taylor, Extraordinary magnetoelasticity and lattice softening in bcc Fe-Ga alloys, J. Appl. Phys. **93**, 8621 (2003).

[13] A. E. Clark, J. B. Restorff, M. Wun-Fogle, D. Wu, and T. A. Lograsso, Temperature dependence of the magnetostriction and magnetoelastic coupling in $Fe_{100-x}Al_x$ ($x = 14.1$, 16.6, 21.5, 26.3) and $Fe_{50}Co_{50}$, J. Appl. Phys. **103**, 07B310 (2008).

[14] M. S. S. Brooks, L. Nordström, and B. Johansson, 3*d*-5*d* band magnetism in rare earth-transition metal intermetallics: Total and partial magnetic moments of the RFe_2 (R = Gd-Yb) Laves phase compounds, J. Phys.: Condens. Matter **3**, 2357 (1991).

[15] M. Richter, Band structure theory of magnetism in 3*d*-4*f* compounds, J. Phys. D: Appl. Phys. **31**, 1017 (1998).

[16] S. Buck and M. Fähnle, Magnetostriction in $TbFe_2$: Weak influence of the internal structural distortion, J. Magn. Magn. Mater. **204**, L1 (1999).

[17] V. I. Gavrilenko and R. Q. Wu, Magnetostriction and magnetism of rare earth intermetallic compounds: First principle study, J. Appl. Phys. **89**, 7320 (2001).

[18] M. Fähnle and F. Welsch, From the electronic structure to the macroscopic magnetic behaviour of rare-earth intermetallics: A combination of *ab initio* electron theory with statistical mechanics and elasticity theory, Physica B **321**, 198 (2002).

[19] H. Wang, Y. N. Zhang, R. Q. Wu, L. Z. Sun, D. S. Xu, and Z. D. Zhang, Understanding strong magnetostriction in $Fe_{100-x}Ga_x$ alloys, Sci. Rep. **3**, 3521 (2013).

[20] U. Atzmony, M. P. Dariel, E. R. Bauminger, D. Lebenbaum, I. Nowik, and S. Ofer, Spin-orientation diagrams and magnetic anisotropy of rare-earth-iron ternary cubic Laves compounds, Phys. Rev. B **7**, 4220 (1973).

[21] N. C. Koon and C. M. Williams, Origins of magnetic anisotropy in cubic RFe_2 Laves phase compounds, J. Appl. Phys. **49**, 1948 (1978).

[22] M. D. Kuz'min, Magnetostriction of $DyFe_2$ and $HoFe_2$: Validity of the single-ion model, J. Appl. Phys. **89**, 5592 (2001).

[23] G. J. Bowden, P. A. J. de Groot, J. D. O'Neil, B. D. Rainford, and A. A. Zhukov, On the anomalous temperature-dependent magnetostriction in intermetallic $DyFe_2$, J. Phys. Condens. Matter **16**, 2437 (2004).

[24] K. N. Martin, P. A. J. de Groot, B. D. Rainford, K. Wang, G. J. Bowden, J. P. Zimmermann, and H. Fangohr, Magnetic anisotropy in the cubic Laves $REFe_2$ intermetallic compounds, J. Phys.: Condens. Matter **18**, 459 (2006).

[25] C. E. Patrick and J. B. Staunton, Crystal field coefficients for yttrium analogues of rare-earth/transition-metal magnets using density-functional theory in the projector-augmented wave formalism, J. Phys.: Condens. Matter **31**, 305901 (2019).

[26] A. Clark, in *Handbook of Ferromagnetic Materials* (Elsevier, 1980), Vol. 1, p. 531.

[27] B. L. Györffy, A. J. Pindor, J. Staunton, G. M. Stocks, and H. Winter, A first-principles theory of ferromagnetic phase transitions in metals, J. Phys. F: Met. Phys. **15**, 1337 (1985).

[28] We note that in a ferrimagnet such as $REFe_2$, the itinerant electron magnetic sublattice may be oriented *antiparallel* to $\hat{\mathbf{e}}$; however, this detail does not affect our discussion, since $E_{\text{itin}}(\hat{\mathbf{e}}, \boldsymbol{\varepsilon}) = E_{\text{itin}}(-\hat{\mathbf{e}}, \boldsymbol{\varepsilon})$.

[29] C. Kittel, Physical theory of ferromagnetic domains, Rev. Mod. Phys. **21**, 541 (1949).

[30] A. Bentouaf, R. Mebsout, H. Rached, S. Amari, A. Reshak, and B. Aïssa, Theoretical investigation of the structural, electronic, magnetic and elastic properties of binary cubic C15-Laves phases TbX_2 (X = Co and Fe), J. Alloys Compd. **689**, 885 (2016).

[31] N. Moulay, H. Rached, M. Rabah, S. Benalia, D. Rached, A. H. Reshak, N. Benkhettou, and P. Ruterana, First-principles calculations of the elastic, and electronic properties of YFe_2, $NiFe_2$ and $YNiFe_4$ intermetallic compounds, Comput. Mater. Sci. **73**, 56 (2013).

[32] M. D. Kuz'min and A. M. Tishin, in *Handbook of Magnetic Materials* (Elsevier, 2008), Vol. 17, p. 149.

[33] G. A. Marchant, C. E. Patrick, and J. B. Staunton, *Ab initio* calculations of temperature-dependent magnetostriction of Fe and *A*2 $Fe_{1-x}Ga_x$ within the disordered local moment picture, Phys. Rev. B **99**, 054415 (2019).

[34] H. Callen and E. Callen, The present status of the temperature dependence of magnetocrystalline anisotropy, and the $l(l+1)/2$ power law, J. Phys. Chem. Solids **27**, 1271 (1966).

[35] M. Loewenhaupt, P. Tils, K. Buschow, and R. Eccleston, Exchange interactions in GdFe compounds studied by inelastic neutron scattering, J. Magn. Magn. Mater. **152**, 10 (1996).

[36] J. S. Griffith, *The Theory of Transition-Metal Ions* (Cambridge University Press, Cambridge, UK, 1961).

[37] C. E. Patrick and J. B. Staunton, Temperature-dependent magnetocrystalline anisotropy of rare earth/transition metal permanent magnets from first principles: The light RCo_5 (R = Y, La-Gd) intermetallics, Phys. Rev. Mater. **3**, 101401 (2019).

[38] J. Sievers, Asphericity of 4*f* -shells in their Hund's rule ground states, Z. Phys. B **45**, 289 (1982).

[39] K. W. H. Stevens, Matrix elements and operator equivalents connected with the magnetic properties of rare earth ions, Proc. Phys. Soc. A **65**, 209 (1952).

[40] A. R. Edmonds, *Angular Momentum in Quantum Mechanics* (Princeton University Press, Princeton, NJ, 1960), Chap. 4, p. 59.

[41] C. J. Bradley and A. P. Cracknell, *The Mathematical Theory of Symmetry in Solids* (Oxford University Press, Oxford, UK, 1972), Chap. 3, p. 82.

[42] S. Kumar, C. E. Patrick, R. S. Edwards, G. Balakrishnan, M. R. Lees, and J. B. Staunton, Torque magnetometry study of the spin reorientation transition and temperature-dependent magnetocrystalline anisotropy in $NdCo_5$, J. Phys.: Condens. Matter **32**, 255802 (2020).

[43] S. Kumar, C. E. Patrick, R. S. Edwards, G. Balakrishnan, M. R. Lees, and J. B. Staunton, Tunability of the spin reorientation transitions with pressure in $NdCo_5$, Appl. Phys. Lett. **116**, 102408 (2020).

[44] M. Lüders, A. Ernst, M. Däne, Z. Szotek, A. Svane, D. Ködderitzsch, W. Hergert, B. L. Györffy, and W. M. Temmerman, Self-interaction correction in multiple scattering theory, Phys. Rev. B **71**, 205109 (2005).

[45] M. Däne, M. Lüders, A. Ernst, D. Ködderitzsch, W. M. Temmerman, Z. Szotek, and W. Hergert, Self-interaction correction in multiple scattering theory: Application to transition metal oxides, J. Phys.: Condens. Matter **21**, 045604 (2009).

[46] These functions have been reported previously in Ref. [25], Fig. 1 and are available on request.

[47] C. E. Patrick, S. Kumar, G. Balakrishnan, R. S. Edwards, M. R. Lees, L. Petit, and J. B. Staunton, Calculating the Magnetic Anisotropy of Rare-Earth/Transition-Metal Ferrimagnets, Phys. Rev. Lett. **120**, 097202 (2018).

[48] C. E. Patrick and J. B. Staunton, Rare-earth/transition-metal magnets at finite temperature: Self-interaction-corrected relativistic density functional theory in the disordered local moment picture, Phys. Rev. B **97**, 224415 (2018).

[49] J. B. Staunton, L. Szunyogh, A. Buruzs, B. L. Gyorffy, S. Ostanin, and L. Udvardi, Temperature dependence of magnetic anisotropy: An *ab initio* approach, Phys. Rev. B **74**, 144411 (2006).

[50] C. E. Patrick, S. Kumar, G. Balakrishnan, R. S. Edwards, M. R. Lees, E. Mendive-Tapia, L. Petit, and J. B. Staunton, Rare-earth/transition-metal magnetic interactions in pristine and (Ni, Fe)-doped YCo_5 and $GdCo_5$, Phys. Rev. Mater. **1**, 024411 (2017).

[51] B. L. Györffy and G. M. Stocks, in *Electrons in Disordered Metals and at Metallic Surfaces*, edited by P. Phariseau and B. Györffy, Nato Science Series B (Springer U.S., 1979), Chap. 4, pp. 89–192.

[52] J. Enkovaara, C. Rostgaard, J. J. Mortensen, J. Chen, M. Dułak, L. Ferrighi, J. Gavnholt, C. Glinsvad, V. Haikola, and H. A. Hansen, *et al.*, Electronic structure calculations

with GPAW: A real-space implementation of the projector augmented-wave method, J. Phys.: Condens. Matter **22**, 253202 (2010).

[53] S. H. Vosko, L. Wilk, and M. Nusair, Accurate spin-dependent electron liquid correlation energies for local spin density calculations: A critical analysis, Can. J. Phys. **58**, 1200 (1980).

[54] A. V. Andreev, in *Handbook of Magnetic Materials*, Vol. 8, edited by K. H. J. Buschow (Elsevier North-Holland, New York, 1995), Chap. 2, p. 59.

[55] G. Wedler, J. Walz, A. Greuer, and R. Koch, The magnetoelastic coupling constant B_2 of epitaxial Fe(001) films, Surf. Sci. **454–456**, 896 (2000).

[56] U. Atzmony, M. P. Dariel, and G. Dublon, Spin-orientation diagram of the pseudobinary $Tb_{1-x}Dy_xFe_2$ Laves compounds, Phys. Rev. B **15**, 3565 (1977).

[57] C. Williams, N. Koon, and B. Das, Torque measurements on single crystal $Dy_xTb_{1-x}Fe_2$ compounds, J. Magn. Magn. Mater. **15-18**, 553 (1980).

[58] U. Atzmony and M. P. Dariel, Nonmajor cubic symmetry axes of easy magnetization in rare-earth-iron Laves compounds, Phys. Rev. B **13**, 4006 (1976).

[59] J. R. Cullen and A. E. Clark, Magnetostriction and structural distortion in rare-earth intermetallics, Phys. Rev. B **15**, 4510 (1977).